Physics of Fluids

RESEARCH ARTICLE | NOVEMBER 01 2024

On the interplay between fluid flow characteristics and small particle deposition in turbulent wall bounded flows

Sanaz Abbasi ; Amirfarhang Mehdizadeh

Physics of Fluids 36, 113305 (2024)
https://doi.org/10.1063/5.0232440

Physics of Fluids ARTICLE pubs.aip.org/aip/pof

On the interplay between fluid flow characteristics and small particle deposition in turbulent wall bounded flows

Cite as: Phys. Fluids **36**, 113305 (2024); doi: 10.1063/5.0232440
Submitted: 7 August 2024 · Accepted: 12 October 2024 ·
Published Online: 1 November 2024

Sanaz Abbasi and Amirfarhang Mehdizadeh[a)]

AFFILIATIONS

School of Science and Engineering, University of Missouri, Kansas City, Missouri 64110, USA

[a)]Author to whom correspondence should be addressed: mehdizadeha@umkc.edu

ABSTRACT

This study investigates the transport and deposition of small particles ($500\,\text{nm} \leq d_p \leq 10\,\mu\text{m}$) in a fully developed turbulent channel flow, focusing on two fluid friction Reynolds numbers: $Re_\tau = 180$ and $Re_\tau = 1000$. Using the point particle–direct numerical simulation method under the assumption of one-way coupling, we study how fluid flow (carrier phase) characteristics influence particle deposition. Our findings suggest that changes in flow conditions can significantly alter the deposition behavior of particles with the same size and properties. Furthermore, we show for the first time that gravity has minimal impact on deposition dynamics only at high Reynolds numbers. This research enhances our understanding of small particle deposition and transport in turbulent flows at high Reynolds numbers, which is crucial for various industrial applications.

I. INTRODUCTION

The transport and deposition of small particles in various industrial and environmental systems, such as the petroleum and petrochemical industries, modern gas turbines, and biomass conversion systems, are critical issues that have drawn significant research attention.[1–5] A comprehensive understanding of the mechanisms behind particle transport and deposition and their interactions is essential for mitigating their negative economic and environmental impacts, such as equipment fouling, reduced efficiency, and harmful emissions. However, despite extensive research, understanding the complex interplay of various mechanisms governing small particles deposition and transport in turbulent flows remains a significant challenge.

The rate of particle deposition, commonly referred to as deposition velocity, is generally expressed as a function of the particle Stokes number, which is the ratio of the particle response time to the characteristic fluid flow timescale. At low Stokes numbers, the dominant deposition mechanism is the Brownian motion, also known as the diffusional regime. As the Stokes number increases, the effect of particle diffusion decreases, yielding to turbophoresis, the convective drift of particles toward the wall induced by the gradient in turbulent intensity, characteristic of the diffusion-impaction regime. With further increases in the Stokes number, particle inertia becomes increasingly significant, leading to the inertia-moderated regime (these regions are demonstrated in Fig. 8).

In our previous study,[6] we demonstrated that the Stokes number alone is insufficient to fully characterize particle deposition; additional parameters such as particle diameter and density also need to be considered, when studying the deposition. Moreover, it was shown that gravity significantly affects the deposition process at low fluid Reynolds number ($Re_\tau = 180$), even for small particles, supporting the findings of Brandt and Coletti.[7]

In addition to particle properties, varying fluid flow characteristics can result in different Stokes numbers for the same particle. Additionally, changes in fluid (carrier phase) Reynolds number alter the flow characteristics such as turbulence intensity, thereby affecting particle transport and deposition. Zhang and Ahmadi[8] examined particle deposition in vertical and horizontal ducts at varying Reynolds numbers, concluding that the effect of gravity varies with flow conditions. However, their study was limited to very low Reynolds numbers and a small number of particles. Similarly, Bernardini[9] investigated particle transport dynamics at different Reynolds numbers but considered solely the drag force, overlooking other forces such as lift, Brownian, and gravity. Consequently, their findings might not be conclusive, particularly for small particles considered in the current study.

This study aims to investigate the effects of flow characteristics on the transport and deposition of small particles. Therefore, point particle–direct numerical simulation (PP–DNS) has been utilized to provide detailed insights into the transport and deposition dynamics

of small particles in a turbulent channel flow at both low ($Re_\tau = 180$) and high ($Re_\tau = 1000$) fluid Reynolds numbers. Furthermore, all relevant forces including drag, lift, gravity, and Brownian are considered. We analyze the deposition dynamics of small particles of varying sizes at these two fluid Reynolds numbers. We further examine the impact of gravity on the deposition dynamics at different fluid Reynolds numbers.

This paper is structured as follows: Sec. II outlines the theoretical framework employed in this study. Section III details the computational domain and the numerical schemes used in the simulations. The results and analyses are presented in Sec. IV. Finally, Sec. V concludes the study and discusses potential future research directions.

II. PHYSICAL BACKGROUND

In this section, we briefly outline the fundamental equations governing turbulent flow dynamics and the equation of motion for particles.

A. Fluid phase

The dimensionless continuity and Navier–Stokes equations for an incompressible, single-phase fluid flow in a channel are given by

$$\nabla \cdot \mathbf{u}^+ = 0, \tag{1}$$

$$\frac{\partial \mathbf{u}^+}{\partial t^+} + \mathbf{u}^+ \cdot \nabla \mathbf{u}^+ = \frac{1}{Re_\tau}\nabla^2 \mathbf{u}^+ - \nabla p^+ + \delta^+_{i,1}, \tag{2}$$

where $\mathbf{u}^+$ and p^+ are the dimensionless fluid velocity and kinematic pressure based on the friction velocity (u_τ) and the channel half-height (h), respectively. Also, $Re_\tau = u_\tau h/\nu$ is the friction Reynolds number, ν is the kinematic viscosity, and $\delta^+_{i,1}$ is a constant pressure gradient driving the flow.

B. Particle tracking

For the study of small particles, we include accelerations due to drag, lift, gravity, and Brownian motion of the particles. Therefore, the dimensionless equations of motion for each individual particle are as follows:

$$\frac{d\mathbf{r}^+_\mathrm{p}}{dt^+} = \mathbf{v}^+_\mathrm{p}, \tag{3}$$

$$\frac{d\mathbf{v}^+_\mathrm{p}}{dt^+} = \mathbf{a}^+_\mathrm{D} + \mathbf{a}^+_\mathrm{L} + \mathbf{a}^+_\mathrm{G} + \mathbf{n}^+_\mathrm{B}, \tag{4}$$

where $\mathbf{r}^+_\mathrm{p}$ and $\mathbf{v}^+_\mathrm{p}$ represent the dimensionless particle position and velocity, respectively. All the variables are dimensionless based on the kinematic viscosity and the friction velocity.

The acceleration due to drag ($\mathbf{a}^+_\mathrm{D}$) including wall modifications for particles moving normal ($C_{\mathrm{DW}\perp}$) or parallel ($C_{\mathrm{DW}\parallel}$) to the wall is expressed as[10,11]

$$\mathbf{a}^+_\mathrm{D} = \frac{\mathbf{u}^+_\mathrm{f} - \mathbf{v}^+_\mathrm{p}}{St}\left(1 + 0.15Re_\mathrm{p}^{0.687}\right)C_\mathrm{DW}, \tag{5}$$

where $\mathbf{u}^+_\mathrm{f}$ is the fluid velocity at particle location and particle Reynolds number is defined as $Re_\mathrm{p} = |\mathbf{u}_\mathrm{f} - \mathbf{v}_\mathrm{p}|d_\mathrm{p}/\nu$. The wall correction factors are given by

$$C_{\mathrm{DW}\parallel} = \left[1 - \frac{9}{16}\left(\frac{d^+_\mathrm{p}}{2l^+_\mathrm{p}}\right) + \frac{1}{8}\left(\frac{d^+_\mathrm{p}}{2l^+_\mathrm{p}}\right)^3 - \frac{45}{256}\left(\frac{d^+_\mathrm{p}}{2l^+_\mathrm{p}}\right)^4 - \frac{1}{16}\left(\frac{d^+_\mathrm{p}}{2l^+_\mathrm{p}}\right)^5\right]^{-1}, \tag{6}$$

$$C_{\mathrm{DW}\perp} = 1 + \frac{9}{8}\left(\frac{d^+_\mathrm{p}}{2l^+_\mathrm{p}}\right) + \left(\frac{9}{8}\frac{d^+_\mathrm{p}}{2l^+_\mathrm{p}}\right)^2, \tag{7}$$

such that l^+_p is the dimensionless distance of the particle from the nearest wall.

The particle Stokes number (St), dimensionless relaxation time, incorporating the Cunningham correction factor (C_c) is defined as:

$$St = \frac{1}{18}\frac{\rho_\mathrm{p}}{\rho}C_c d^{+2}_\mathrm{p}, \tag{8}$$

$$C_c = 1 + \frac{2\lambda}{d_\mathrm{p}}\left(1.257 + 0.4e^{-1.1\frac{d_\mathrm{p}}{2\lambda}}\right), \tag{9}$$

where ρ is the fluid density and d_p and ρ_p are particle diameter and density. Chen and McLaughlin[12] showed that considering the Cunningham correction factor is important in deposition of submicron particles ($d_p \leq 1\,\mu$m).

The acceleration due to lift ($\mathbf{a}^+_\mathrm{L}$) includes shear-lift and wall-induced lift. Here, the shear-lift model is based on the Saffman lift[13] with a correction (J_L) proposed by Mei[14] and the wall-induced lift is calculated according to the model presented by Takemura and Magnaudet.[15] The lift acceleration is given by

$$\mathbf{a}^+_\mathrm{L} = 0.1714J_\mathrm{L}\frac{1}{\frac{\rho_\mathrm{p}}{\rho}d^+_\mathrm{p}}|\mathbf{u}^+_\mathrm{f} - \mathbf{v}^+_\mathrm{p}|\sqrt{\boldsymbol{\omega}^+}\frac{\left(\mathbf{u}^+_\mathrm{f} - \mathbf{v}^+_\mathrm{p}\right)\times\boldsymbol{\omega}^+}{|\mathbf{u}^+_\mathrm{f} - \mathbf{v}^+_\mathrm{p}||\boldsymbol{\omega}^+|} + \frac{3}{4}\frac{1}{\frac{\rho_\mathrm{p}}{\rho}d^+_\mathrm{p}}V^{+\,2}_\mathrm{LW}C_\mathrm{LW}, \tag{10}$$

where

$$J_\mathrm{L} = 0.3\left(1 + \tanh\left[\frac{5}{2}\left(\log_{10}\varepsilon + 0.191\right)\right]\right)\left(\frac{2}{3} + \tanh(6\varepsilon - 1.92)\right), \tag{11}$$

$$\varepsilon = \frac{\sqrt{\boldsymbol{\omega}^+}}{|\mathbf{u}^+_\mathrm{f} - \mathbf{v}^+_\mathrm{p}|}, \tag{12}$$

$$C_\mathrm{LW} = C_\mathrm{LW0}\left(1 + 0.6Re^{0.5}{}_\mathrm{LW} - 0.55Re^{0.08}_\mathrm{LW}\right)^2\left(\frac{1}{3}\frac{2l^+_\mathrm{p}}{d^+_\mathrm{p}}\right)^{-2\tanh(0.01Re_\mathrm{LW})}, \tag{13}$$

$$C_\mathrm{LW0} = \begin{cases}\left[\frac{9}{8} + 5.78\times10^{-6}z^{*4.58}\right]\exp(-0.292z^*) & \text{for } z^* \leq 10,\\ 8.94(z^*)^{-2.09} & \text{for } z^* > 10,\end{cases} \tag{14}$$

$$V_\mathrm{LW} = \left(\left[u_{x,\mathrm{f}} - v_{x,\mathrm{p}}\right]^2 + \left[u_{y,\mathrm{f}} - v_{y,\mathrm{p}}\right]^2\right)^{0.5}, \tag{15}$$

$$Re_\mathrm{LW} = V_\mathrm{LW}d_\mathrm{p}/\nu, \tag{16}$$

$$z^* = z_\mathrm{p}V_\mathrm{LW}/\nu. \tag{17}$$

A detailed description of these equations can be found in our previous work.[6]

Brownian motion of particles, denoted by $\mathbf{n}_B^+$, is modeled as a Gaussian white noise ($\mathbf{G}$),

$$\mathbf{n}_B^+ = \mathbf{G}\sqrt{\frac{\pi S_0^+}{\Delta t^+}}, \tag{18}$$

with a spectral density (S_0^+) given by

$$S_0^+ = \frac{2}{\pi Sc St^2}. \tag{19}$$

The Schmidt number, Sc, is defined as the ratio of kinematic viscosity to the Brownian diffusivity (D),

$$Sc = \frac{\nu}{D} = \frac{3\pi\nu d_p \mu}{C_c k T}, \tag{20}$$

where T is the absolute temperature of the media, μ is the dynamic viscosity of the fluid, and $k = 1.38 \times 10^{-23}$ J/°k is the Boltzmann constant.[16,17]

The gravitational acceleration ($\mathbf{a}_G^+$) accounting for Buoyancy effects is defined as follows:

$$\mathbf{a}_G^+ = \left(1 - \frac{1}{\frac{\rho_p}{\rho}}\right)\mathbf{g}^+, \tag{21}$$

where $\mathbf{g}^+$ is the dimensionless gravitational acceleration with the absolute magnitude of 0.0546.

Here, the deposition velocity is defined as the particle flow rate on the wall normalized by the total number of particles per unit area and is calculated as[6]

$$u_d^+ = \frac{\Delta N_{dep} H^+}{N_0 \Delta t^+}, \tag{22}$$

where ΔN_{dep} represents the number of particles deposited on the wall within a time interval (Δt^+), H^+ is the half-height of the channel in dimensionless units, and N_0 is the initial number of particles.

III. COMPUTATIONAL SETUP

In this section, we describe the details of our computations and the test cases.

A. Carrier phase

In this study, direct numerical simulations (DNSs) are conducted for two flow configurations at $Re_\tau = 180$ and $Re_\tau = 1000$. The incompressible Navier–Stokes equations are solved using a second-order finite difference method, called **CaNS** (Canonical Navier–Stokes).[18] Flow is driven by a constant pressure gradient, as detailed in Eq. (2), and it is integrated in time with a three-step Runge–Kutta scheme (RK3). Periodic boundary conditions are applied in the streamwise and spanwise directions, while a no-slip condition is used in the wall-normal direction. The computational domain dimensions are $4\pi h \times 2\pi h \times 2h$ along the streamwise, spanwise, and wall-normal directions, respectively, with $h = 2$ cm (channel half-height). The fluid is considered as air with a viscosity of $\nu = 1.57 \times 10^{-5}$ m^2/s. Details of the domain discretization for each flow case are provided in Fig. 1 and Table I.

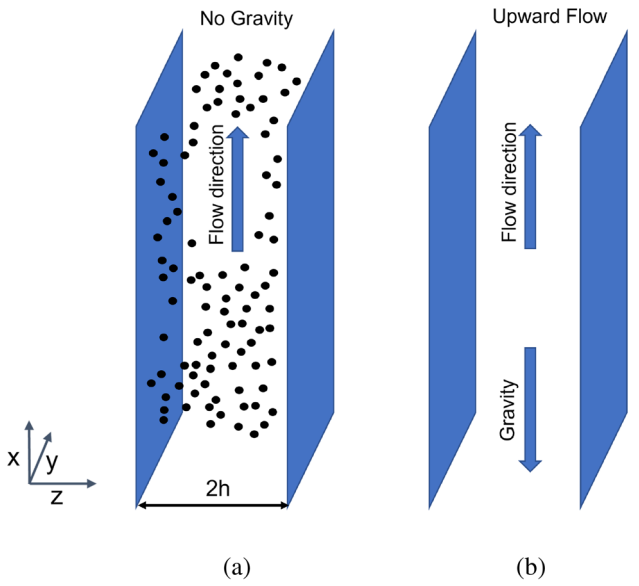

FIG. 1. A schematic of the computational domain for a channel at (a) zero gravity and (b) upward flow in the opposite direction of gravity.

B. Particle phase

To investigate particle transport and deposition, the CaNS code is integrated with a Lagrangian Particle Tracking (LPT) solver, assuming a dilute system, i.e., the particle motion does not influence the fluid flow. The time integration for the particle phase utilizes a second-order Runge–Kutta scheme, similar to the fluid phase. The fluid information such as velocity and vorticity at each particle location are determined through the trilinear interpolation method. Previously, it is mentioned that this interpolation method is sufficiently accurate for PP-DNS.[6] In each simulation, 10^5 particles are injected into the domain at random locations and assigned velocities based on the interpolated fluid fields at their respective positions.

Similarly, periodic boundary conditions are applied in the streamwise and spanwise directions, such that particles exiting the

TABLE I. Details on the computational domain and particle properties.

Re_τ	Number of grid points[a]	Δt^+[b]	$\frac{\rho_p}{\rho}$	d_p(m)	St
180	$512 \times 256 \times 144$	0.125	2000	5×10^{-7}	2×10^{-3}
				1×10^{-6}	1×10^{-2}
				5×10^{-6}	2.2×10^{-1}
				10×10^{-6}	1
1000	$2048 \times 1536 \times 448$	0.11	2000	5×10^{-7}	7×10^{-2}
				1×10^{-6}	2.8×10^{-1}
				5×10^{-6}	7
				10×10^{-6}	28

[a]Streamwise × spanwise × wall-normal.
[b]Fluid phase time step.

domain on one side re-enter from the opposite side. Furthermore, a sticky system is considered in this study, i.e., particles are considered as deposited and removed from the domain when their distance to the wall falls below their radius. To maintain a constant particle count during the simulation, a new particle is introduced at a random location whenever a particle is deposited and removed. This framework has been validated in our previous investigation.[6] We also note that the time step is selected to be an order of magnitude smaller than the particle relaxation time, following the criterion proposed in Ounis *et al.*[19] for accurate sense of Brownian force.

As previously discussed, particle deposition is a multi-dimensional phenomenon influenced by various parameters and cannot be described solely by the Stokes number.[6] The Stokes number itself is influenced by factors such as particle diameter, particle density, and the Kolmogorov length scale of the fluid phase, depending on the specific configuration and Reynolds number. In our prior study, we investigated the effect of particle characteristics on the deposition rate and found that particles of varying diameters and densities, even at identical Stokes numbers, exhibited different deposition rates.[6] Our findings also indicated that at low fluid Reynolds number ($Re_\tau = 180$), gravitational effects significantly alter the deposition rate and zero-gravity conclusions cannot be extrapolated to non-zero-gravity configurations.[7]

This study aims to advance our understanding of small particle transport and deposition at high fluid Reynolds numbers relevant to industrial applications and to assess the impact of gravity on the deposition process at such high fluid Reynolds numbers. To achieve this, we carry out two sets of simulations for each particle: one under zero-gravity conditions and one with gravity, at both low and high Reynolds numbers. For simulations including gravity, it is assumed that the fluid flow opposes the direction of gravity, i.e., an upward flow. A summary of the fluid and particle properties is provided in Fig. 1 and Table I.

IV. RESULTS

In this section, we analyze the influence of the fluid Reynolds number on particle statistical quantities and its interplay with gravity on particle deposition. To calculate particle statistics, the computational domain is discretized into $N_s = 151$ slabs along the wall-normal direction. The statistical data are first ensemble-averaged, followed by time-averaging. The center of each slab is determined using hyperbolic-tangent binning,[20] with a stretching factor of $\gamma = 2.0$,

$$\Delta z^+(s) = \frac{Re_\tau}{\tanh\gamma}\left[\tanh\left(\gamma\frac{s}{N_s}\right) - \tanh\left(\gamma\frac{s-1}{N_s}\right)\right]. \quad (23)$$

Data collection begins after the particle distribution has reached almost fully developed state. The steady-state distribution of particles can be quantified by calculating the Shannon entropy (S).[21] The Shannon entropy is defined as the probability of finding a particle in a given slab, $p_i = N_i/N_t$, and is expressed as

$$S = \frac{-\sum_{i=1}^{N_s} p_i \ln p_i}{\ln N_s}, \quad (24)$$

where N_i represents the instantaneous number of particles in slab i, and N_t denotes the total number of particles within the entire computational domain. Figure 2 illustrates the temporal evolution of Shannon entropy for the smallest ($d_p = 500$ nm) and largest ($d_p = 10\,\mu$m) particles at both low and high Reynolds numbers with zero-gravity setting. All cases approach a nearly fully developed state by the dimensionless time of $t^+ = 1500$.

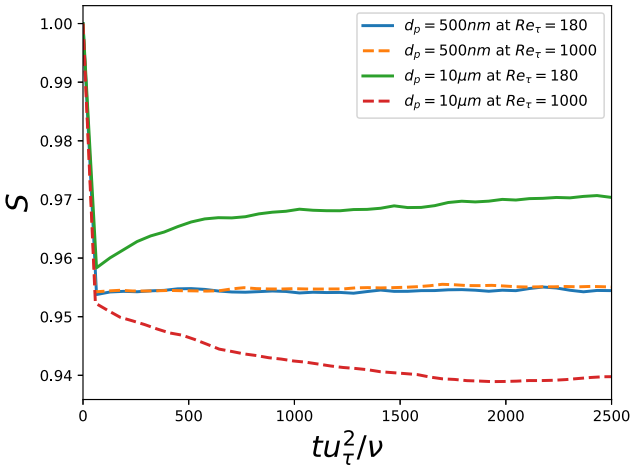

FIG. 2. Time evolution of Shannon entropy for the smallest ($d_p = 500$ nm) and largest ($d_p = 10\,\mu$m) particles at low ($Re_\tau = 180$) and high ($Re_\tau = 1000$) Reynolds number.

To compare the particle statistics under zero-gravity and an upward flow at two different Reynolds numbers, Fig. 3 presents the mean particle concentration across the channel. It is observed that under zero-gravity condition, the mean concentration increases with rising fluid velocity (Reynolds number) for all particle sizes. This change can be attributed to the fact that the Stokes number is dependent on both particle properties as well as fluid characteristics. Therefore, when the fluid Reynolds number, i.e., friction velocity, increases, the particle Stokes number increases as well. Consequently, this leads to an increased effect of particle impaction, which pushes the particles toward the wall. Furthermore, as the fluid Reynolds number increases, the drag force (the dominant force) in the near-wall region significantly decreases, which also contributes to higher particle concentration. A detailed discussion of the forces/accelerations is provided later in the text. Comparing the concentrations for the largest particle ($d_p = 10\,\mu$m) in Fig. 3(d) at two fluids Reynolds numbers, the slight increase at the higher Reynolds number is due to the significant simultaneous increase in the deposition rate (6 orders of magnitude). Since the particles are removed when deposited and reintroduced randomly in the channel, the near-wall concentration shows only a slight increase instead of a substantial increase.

When comparing the particle concentrations under zero-gravity and non-zero gravity conditions, a slight increase is noted for the smaller particles [$d_p = 500$ nm and 1 μm in Figs. 3(a) and 3(b)] at low Reynolds number. The reason for this is likely the relatively small size of the particles, which makes them more susceptible to Brownian motion and less influenced by gravitational settling. However, for larger particles [$d_p = 5\,\mu$m and 10 μm in Figs. 3(c) and 3(d)] at $Re_\tau = 180$, there is a substantial change in the near-wall concentration, and the particles are pushed away from the wall, as previously discussed in Ref. 6. This particle size range may mark a transition where

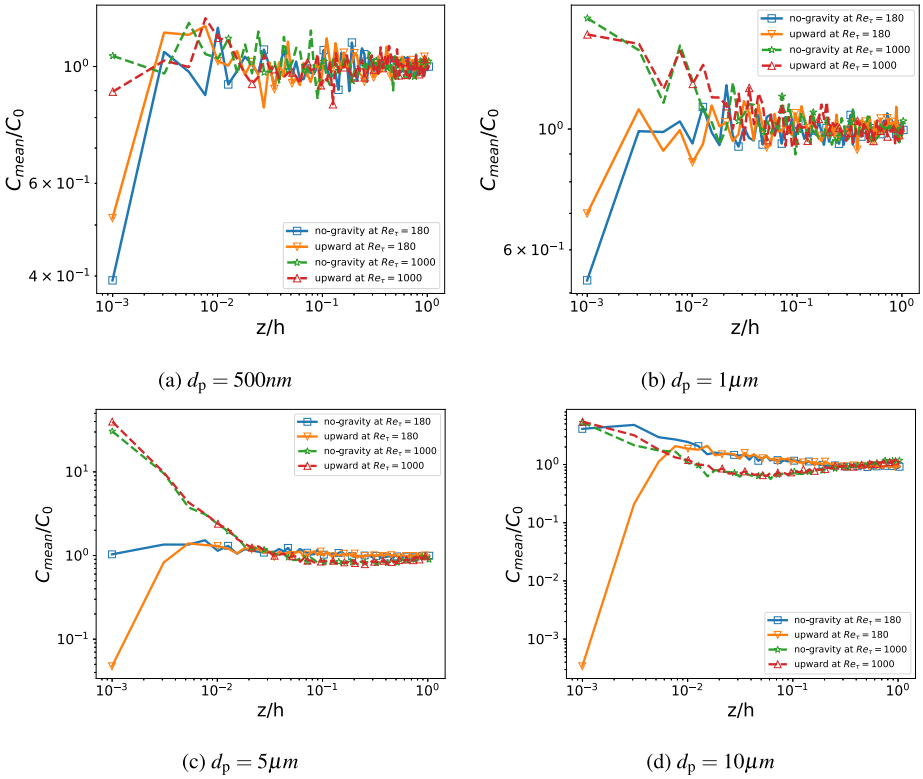

(a) $d_p = 500nm$ (b) $d_p = 1\mu m$

(c) $d_p = 5\mu m$ (d) $d_p = 10\mu m$

FIG. 3. Mean concentration profile at zero gravity for (a) $d_p = 500$ nm, (b) $d_p = 1\ \mu$m, (c) $d_p = 5\ \mu$m, and (d) $d_p = 10\ \mu$m. Higher Reynolds number increases the near-wall particle concentration due to impaction.

gravitational effect starts to play a more significant role at low Reynolds number ($Re_\tau = 180$). Conversely, at $Re_\tau = 1000$, gravity does not have any considerable effect on particle concentration or deposition velocity. This finding suggests that the influence of gravity on particle transport and deposition dynamics may be negligible only at high Reynolds number dispersed flows.

To support our findings, we present the mean streamwise velocity of the particles in Fig. 4. For the smaller particles [Figs. 4(a) and 4(b)], the particle velocity closely follows the fluid velocity. However, for the larger particles [Figs. 4(c) and 4(d)], there is a noticeable deviation from the underlying fluid velocity, particularly at the higher Reynolds number. This deviation is attributed to the larger inertia of bigger particles with the increase of friction velocity and consequently the Stokes number, which prevents them from fully responding to the fluid flow changes.

Interestingly, the presence of gravity does not significantly affect the mean streamwise velocity of the particles at either Reynolds number and alters it slightly only in the near-wall region. This can be explained by the fact that at low Reynolds number, the particle sizes and Stokes numbers are still small enough to closely follow the fluid flow. However, at the higher fluid Reynolds number, the particle inertia dominates over gravity, which leads to a negligible impact of gravity on the particle velocities. This observation aligns with the minimal changes in particle concentration profiles at high Reynolds numbers in Fig. 3.

In our previous work,[6] we demonstrated that root mean square (RMS) of wall-normal particle velocity plays an important role in the deposition process of small particles. We present the RMS of streamwise and wall-normal velocity in Figs. 5 and 6. At low fluid Reynolds number, for the smallest particle [Figs. 5(a) and 6(a)], although the particle velocity does not show any deviation from the fluid, Brownian diffusion can influence the velocity variance in the near-wall region, thereby higher deposition velocity in comparison to the other particle sizes. This effect reduces as the particle size increases, and the variance of particle velocity approaching the laden fluid [Figs. 5(b)–5(d) and 6(b)–6(d)].

Furthermore, the effect of Brownian diffusion decreases as the fluid velocity increases due to higher Stokes numbers, while the influence of turbophoresis becomes more pronounced. Especially at the higher Reynolds number, for the smaller particles [Figs. 5(a) and 5(b) and 6(a) and 6(b)], the near-wall deviation from the laden fluid represents the diffusion-impaction regime, while for larger particles [Figs. 5(c) and 5(d) and 6(c) and 6(d)], particle inertia gets dominant and the particle relaxation time increases and, consequently, the greater deviation from laden fluid is observed. This behavior clearly demonstrates how flow characteristics contribute to variations in particle velocity variances, which in turn determine the deposition rates of small particles. For both Reynolds numbers, gravity does not change the velocity variances considerably.

Figure 7 demonstrates the accelerations in the wall-normal direction for the smallest ($d_p = 500$ nm) and largest ($d_p = 10\ \mu$m) particles. At low Reynolds number, the drag acceleration is higher due to the smaller Stokes number compared to the higher Reynolds number. As expressed in Eq. (5), drag acceleration is inversely proportional to the Stokes number. Thus, drag acceleration decreases with either an increase in particle size and density or an increase in fluid friction velocity, as depicted in Figs. 7(a) and 7(b).

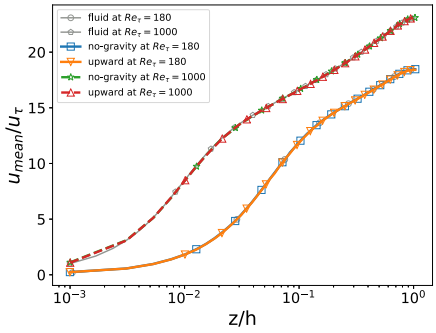

(a) $d_p = 500nm$

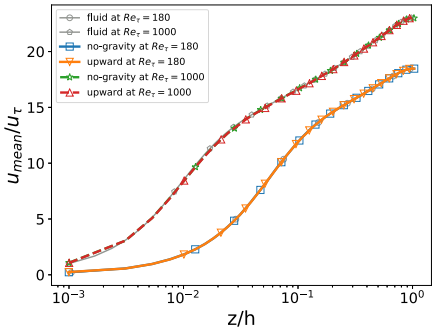

(b) $d_p = 1\mu m$

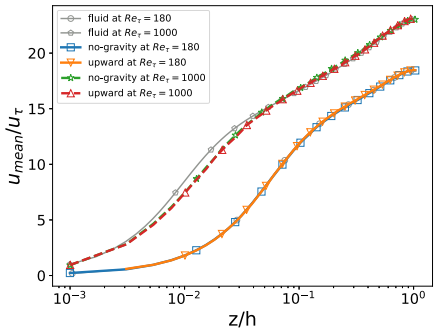

(c) $d_p = 5\mu m$

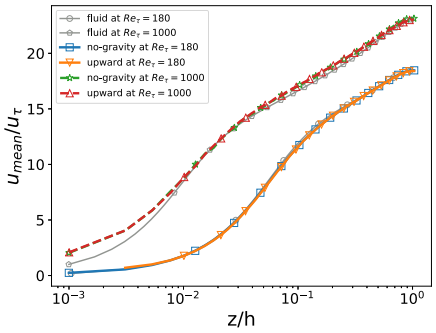

(d) $d_p = 10\mu m$

FIG. 4. Mean streamwise velocity profile for (a) $d_p = 500$ nm, (b) $d_p = 1\,\mu$m, (c) $d_p = 5\,\mu$m, and (d) $d_p = 10\,\mu$m. Smaller particles follow the fluid velocity, while the larger particles deviate from the underlying fluid velocity at higher Reynolds number.

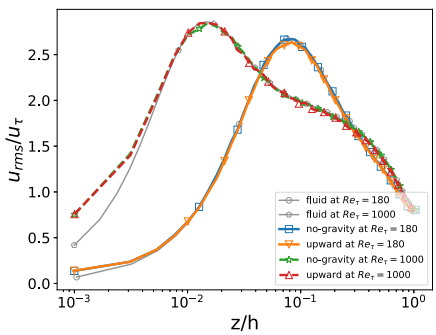

(a) $d_p = 500nm$

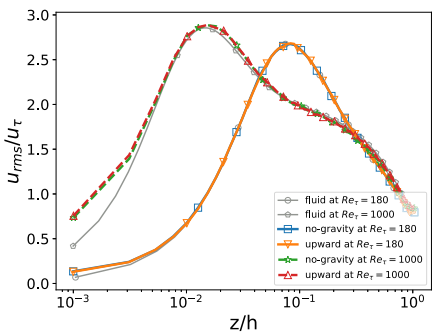

(b) $d_p = 1\mu m$

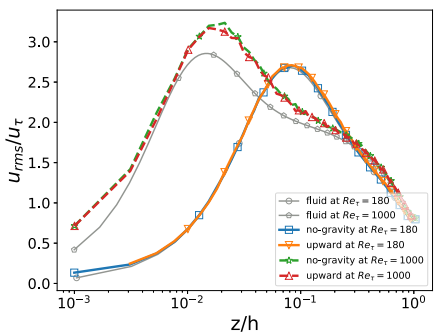

(c) $d_p = 5\mu m$

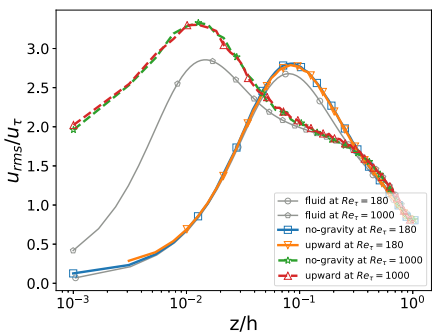

(d) $d_p = 10\mu m$

FIG. 5. RMS of streamwise velocity profile for (a) $d_p = 500$ nm, (b) $d_p = 1\,\mu$m, (c) $d_p = 5\,\mu$m, and (d) $d_p = 10\,\mu$m. The near-wall deviation from the laden fluid increases with increase in the Reynolds number.

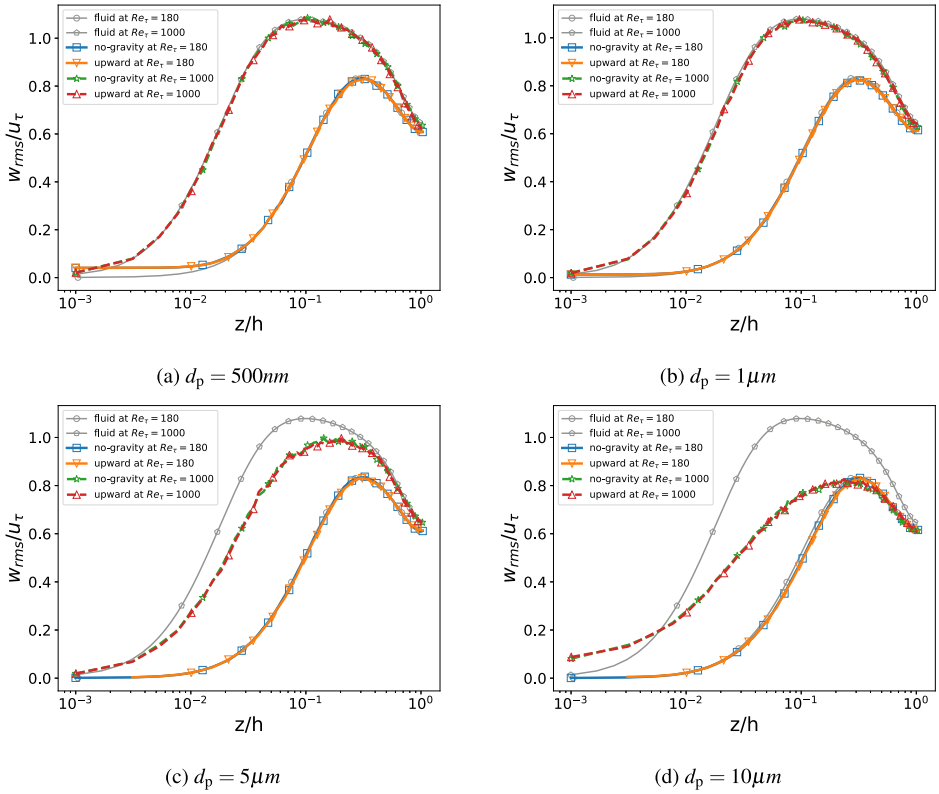

(a) $d_p = 500nm$ (b) $d_p = 1\mu m$

(c) $d_p = 5\mu m$ (d) $d_p = 10\mu m$

FIG. 6. RMS of wall-normal velocity profile: (a) $d_p = 500$ nm, (b) $d_p = 1\ \mu$m, (c) $d_p = 5\ \mu$m, and (d) $d_p = 10\ \mu$m.

According to Eq. (10), lift acceleration is influenced by both the Stokes number and dimensionless particle size (particle diameter). Moreover, gravity affects the particle streamwise velocity and consequently lift in the wall-normal direction.[6] Ultimately this could lead to small alterations in the deposition dynamics. Such impacts are more pronounced at low fluid Reynolds numbers.[6] Therefore, at higher fluid Reynolds numbers lift and consequently the deposition rate remain unaffected as shown in Figs. 7(c) and 7(d).

The Brownian acceleration diminishes with increasing particle size and Stokes number, as noted in Eq. (18). For the smaller particle at low fluid Reynolds number [Fig. 7(e)], the order of Brownian acceleration is the same as the drag acceleration, however, at the higher Reynolds number, the order of magnitude of Brownian reduces to the same order as lift, significantly smaller than drag. For the larger particle [Fig. 7(f)], the effect of Brownian motion is very small in comparison to other accelerations at low fluid Reynolds number and diminishes completely at the higher fluid Reynolds number. Our findings confirm the remark of Li and Ahmadi[17] that the effect of Brownian motion can be neglected for particles larger than 1 μm.[22]

Figure 8 illustrates the deposition velocity with respect to the Stokes number. At low fluid Reynolds numbers, gravity enhances the deposition velocity for the smallest particle ($d_p = 500$ nm) due to slight increase in accelerations toward the wall. Conversely, for larger particles, substantial positive lift prevents proximity to the wall, thus preventing the deposition [see Fig. 7(d)]. As the fluid friction velocity increases, the Stokes number and consequently the influence of impaction also rises, leading to an increase in deposition velocity for particles of the same size. It is further observed that gravity does not affect the deposition velocity substantially at the (fluid) higher Reynolds numbers.

To provide a visual representation of the variations in the deposition process, Fig. 9 displays the number of particles in the deposition region [$O(d_p)$] at $t^+ = 1500$ for particle size of 5 μm. It can be observed that at lower Reynolds number when the effect of gravity is included (represented by red points), the number of particles in the near-wall region reduces significantly. However, at higher Reynolds number, the number of particles in the near-wall region is notably greater and, consequently, the deposition velocity is higher. Conversely, inclusion of gravitational effect does not have any impact on the particle deposition rate at the higher Reynolds number.

Figure 10 depicts the variation in deposition velocity for upward flows at both low and high fluid Reynolds numbers with respect to particle diameter. Notably, the deposition velocity increases significantly for larger particles ($d_p = 5$ and 10 μm) as they transition from the diffusion regime at the lower fluid Reynolds number to the impaction regime at the higher fluid Reynolds number, thereby altering the deposition rate considerably.

This indicates that for a comprehensive study of deposition, both flow characteristics and particle properties must be considered, as the Stokes number alone may not fully capture the deposition mechanism.

V. CONCLUSION AND OUTLOOK

This study investigated the influence of the fluid (carrier phase) Reynolds number and gravity on particle transport and deposition in a turbulent channel flow by performing PP-DNSs at two fluid Reynolds numbers ($Re_\tau = 180$ and 1000) for small particle sizes. Furthermore,

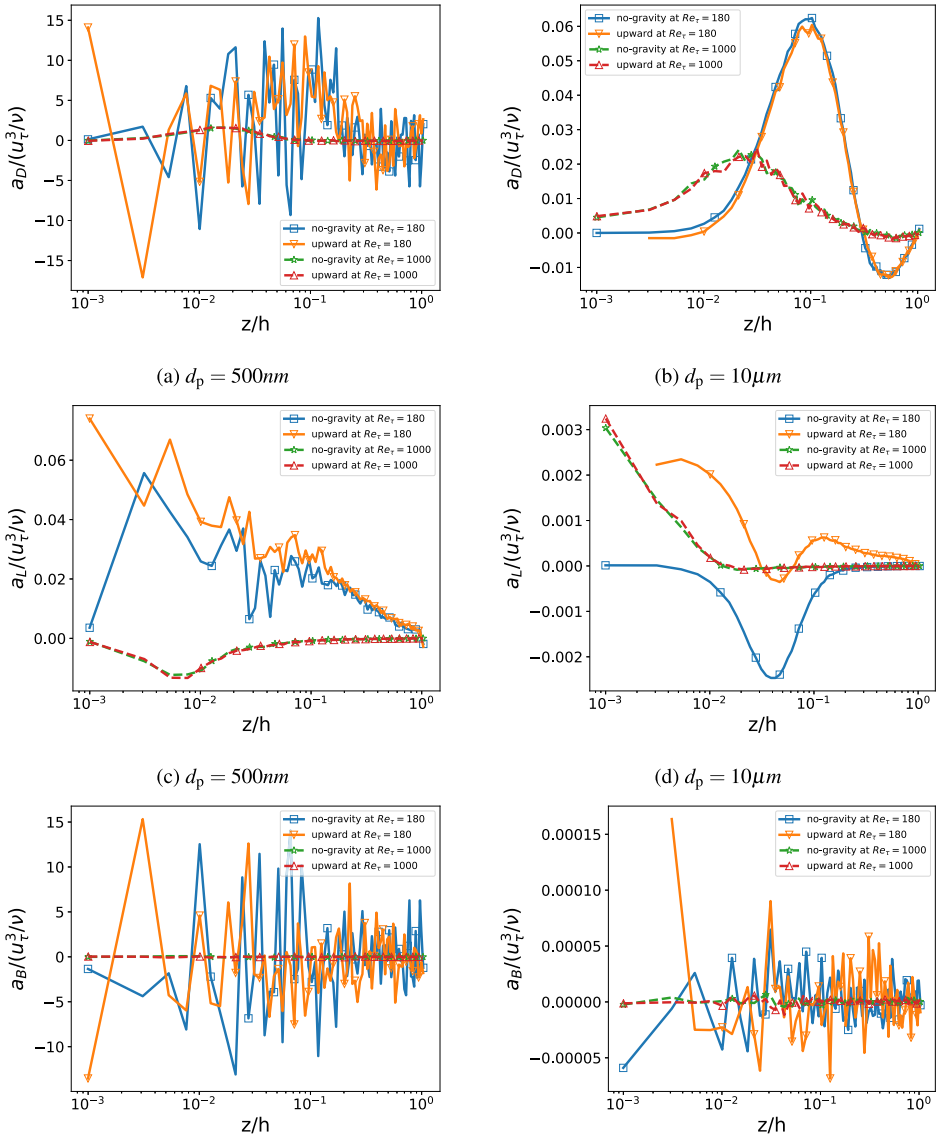

(a) $d_p = 500nm$ (b) $d_p = 10\mu m$

(c) $d_p = 500nm$ (d) $d_p = 10\mu m$

(e) $d_p = 500nm$ (f) $d_p = 10\mu m$

FIG. 7. Profiles of drag for (a) $d_p = 500$ nm and (b) $d_p = 10\,\mu$m, lift for (c) $d_p = 500$ nm and (d) $d_p = 10\,\mu$m, and Brownian for (e) $d_p = 500$ nm and (d) $d_p = 10\,\mu$m in the wall-normal direction. The effect of gravity is negligible at high Reynolds number.

we explored the interplay between fluid Reynolds number, gravity, and the deposition process.

At the lower fluid Reynolds number ($Re_\tau = 180$), Brownian diffusion is the dominant mechanism responsible for deposition, particularly affecting smaller particles, leading to higher deposition velocities in comparison to larger particle sizes. Conversely, for larger particles getting close to the diffusion-impaction regime, the deposition velocity decreases. At higher fluid Reynolds number ($Re_\tau = 1000$), the increased fluid velocity enhances turbophoresis and, consequently, the deposition rate. On the other hand, gravity's role in particle deposition varies with particle size and fluid Reynolds number. For smaller particles ($d_p = 500$nm), gravity slightly increases the deposition rate at low fluid Reynolds numbers, primarily through changes in accelerations (see Fig. 7). However, for larger particles ($d_p = 5\mu$m and $d_p = 10\mu$m), gravity significantly reduced the near-wall concentration and deposition rate via the change in particle streamwise velocity and subsequently lift that causes particles to be pushed away from the wall. At the higher fluid Reynolds number, the effect of gravity becomes negligible, indicating that particle inertia dominates gravitational settling.

In summary, two main conclusions can be drawn based on the results of this work:

(1) Fluid (carrier phase) Reynolds number, i.e., fluid flow characteristics, have a significant effect on the deposition process of small particles with same characteristics. One could observe the transition from diffusion to diffusion-impaction and then

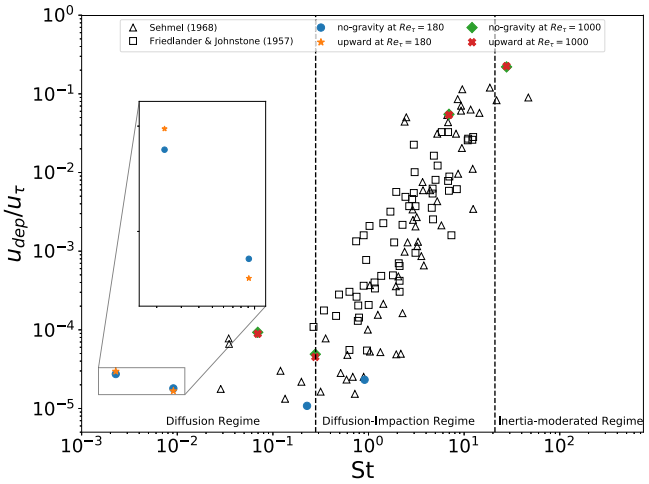

FIG. 8. Deposition velocity vs Stokes number at both fluid Reynolds numbers. The deposition regime changes with increase in either particle size or fluid friction velocity. The experimental data are taken from Young and Leeming.[23]

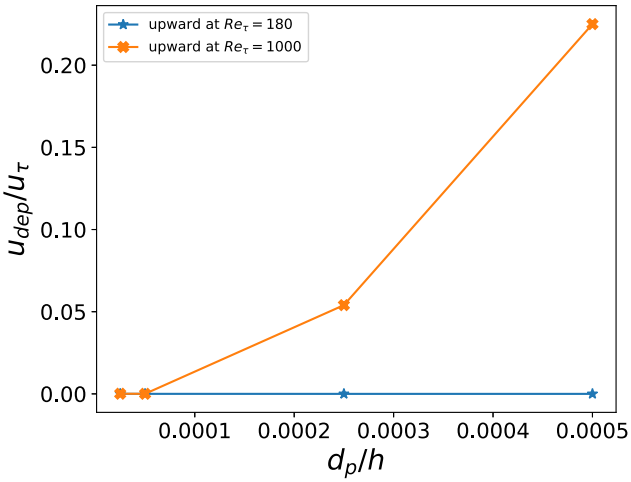

FIG. 10. Deposition velocity vs particle diameter ratio to half-channel height at both fluid Reynolds numbers. The deposition velocity increases considerably at the higher Reynolds number for the larger particles.

inertia-moderated regimes, due to change in fluid Reynolds number, particularly for larger particles.

(2) Considering gravity is crucial at low fluid Reynolds numbers, which is in agreement with the previous findings,[6–8] and it can only be neglected at high fluid Reynolds numbers consistent with findings in Young and Leeming.[23] However, our findings are applicable when small particles are considered (less than 10 μm), and the role of gravity in the deposition process cannot be generalized for larger particles.

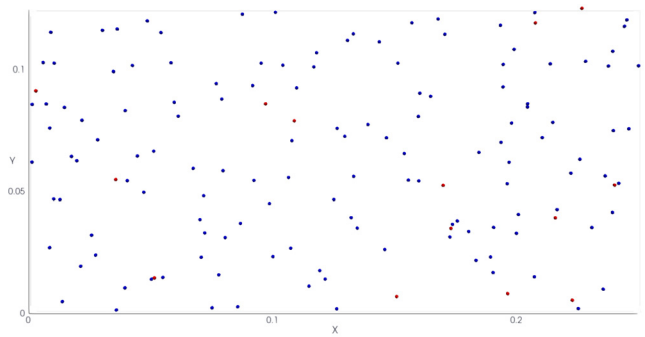

(a) $Re_\tau = 180$

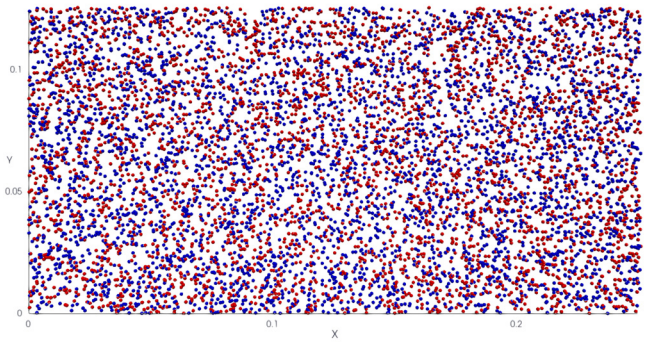

(b) $Re_\tau = 1000$

FIG. 9. The number of particles in the near-wall region at (a) $Re_\tau = 180$ and (b) $Re_\tau = 1000$ at time $t^+ = 1500$ for $d_p = 5\,\mu$m. The blue points are particles at zero-gravity setting and the red points are the particles at the upward flow.

Finally, our study indicates the complex dynamics of particle deposition, and underscores the importance of considering multiple factors, including Stokes number, particle properties, and flow conditions, to predict and control particle deposition in practical applications.

In this investigation, as previously discussed, we postulated that the presence of particles does not have a significant influence on the fluid flow dynamics. However, an increase in either the number or the size of particles leads to an increase in the volume fraction of the dispersed phase. This necessitates the incorporation of the interactions between the particles and the continuous phase (two-way coupling) as well as the consideration of particle collisions (four-way coupling), where the particle size is larger than the Kolmogorov length scale. Empirical evidence suggests that the dispersed phase can mitigate the turbulence intensity within the flow regime when large particles are considered.[24,25] This attenuation of turbulence may consequently result in a decrease in particle deposition rates since strong correlations between sweep events—characterized by high-speed fluid motion toward the wall (turbophoresis)—and the flux of particles toward the wall are recognized as a primary mechanism driving deposition processes. Johnson *et al.*[26] also investigated the influence of volume fraction on particle concentration; while their study did not specifically address particle deposition, it was observed that an increase in volume fraction correlates with a reduction in near-wall particle concentration. This observation similarly implies a potential decrease in particle deposition rates where the dilute system assumption becomes invalid. Further investigation into these dynamics, particularly when small particles are considered, and their implications for the particle deposition process is essential and merits attention in future research efforts.

ACKNOWLEDGMENTS

This work is supported by the National Science Foundation/CBET, Award No. 2219446. Additionally, the computational time was provided by NCSA Delta CPU at University of Illinois Urbana–Champaign and Rockfish at Johns Hopkins University through allocation "MCH240014" from the Advanced Cyberinfrastructure Coordination Ecosystem: Services & Support (ACCESS) program, which is supported by National Science Foundation Grant Nos. 2138259, 2138286, 2138307, 2137603, and 2138296.[27]

AUTHOR DECLARATIONS

Conflict of Interest

The authors have no conflicts to disclose.

Author Contributions

Sanaz Abbasi: Conceptualization (equal); Data curation (lead); Formal analysis (equal); Investigation (lead); Methodology (lead); Resources (equal); Software (lead); Validation (lead); Visualization (lead); Writing – original draft (equal). **Amirfarhang Mehdizadeh:** Conceptualization (equal); Formal analysis (equal); Funding acquisition (lead); Resources (equal); Supervision (lead); Writing – original draft (equal).

DATA AVAILABILITY

The data that support the findings of this study are available from the corresponding author upon reasonable request.

REFERENCES

[1]S. Alimohammadi, S. Zendehboudi, and L. James, "A comprehensive review of asphaltene deposition in petroleum reservoirs: Theory, challenges, and tips," Fuel **252**, 753–791 (2019).
[2]H. Lu and Y. Wang, "Particle deposition in ventilation ducts: A review," Build. Simul. **12**, 723–734 (2019).
[3]L. Alcoforado, A. Ari, J. de Melo Barcelar, S. C. S. Brandão, J. B. Fink, and A. D. de Andrade, "Impact of gas flow and humidity on trans-nasal aerosol deposition via nasal cannula in adults: A randomized cross-over study," Pharmaceutics **11**, 320 (2019).
[4]V. K. H. Bui, J. Moon, M. Chae, D. Park, and Y. Lee, "Prediction of aerosol deposition in the human respiratory tract via computational models: A review with recent updates," Atmosphere **11**, 137 (2020).
[5]M. Sommerfeld, O. Sgrott, M. Taborda, P. Koullapis, K. Bauer, and S. Kassinos, "Analysis of flow field and turbulence predictions in a lung model applying RANS and implications for particle deposition," Eur. J. Pharm. Sci. **166**, 105959 (2021).
[6]S. Abbasi and A. Mehdizadeh, "A computational study on the effect of particle characteristics on the deposition of small particles in turbulent wall-bounded flows," Int. J. Multiphase Flow **174**, 104754 (2024).
[7]L. Brandt and F. Coletti, "Particle–laden turbulence: Progress and perspectives," Annu. Rev. Fluid Mech. **54**, 159–189 (2022).
[8]H. Zhang and G. Ahmadi, "Aerosol particle transport and deposition in vertical and horizontal turbulent duct flows," J. Fluid Mech. **406**, 55–80 (2000).
[9]M. Bernardini, "Reynolds number scaling of inertial particle statistics in turbulent channel flows," J. Fluid Mech. **758**, R1 (2014).
[10]H. Faxen, "Die bewegung einer starren kugel langs der achse eines mit zaher flussigkeit gefullten rohres," Arkiv Mat. Astron. Fys. **17**, 1–28 (1923).
[11]A. D. Maude, "The movement of a sphere in front of a plane at low Reynolds number," Br. J. Appl. Phys. **14**, 894 (1963).
[12]M. Chen and J. B. McLaughlin, "A new correlation for the aerosol deposition rate in vertical ducts," J. Colloid Interface Sci. **169**, 437–455 (1995).
[13]P. G. Saffman, "The lift on a small sphere in a slow shear flow," J. Fluid Mech. **22**, 385–400 (1965).
[14]R. Mei, "An approximate expression for the shear lift force on a spherical particle at finite Reynolds number," Int. J. Multiphase Flow **18**, 145–147 (1992).
[15]F. Takemura and J. Magnaudet, "The transverse force on clean and contaminated bubbles rising near a vertical wall at moderate Reynolds number," J. Fluid Mech. **495**, 235–253 (2003).
[16]H. Ounis and G. Ahmadi, "A comparison of Brownian and turbulent diffusion," Aerosol Sci. Technol. **13**, 47–53 (1990).
[17]A. Li and G. Ahmadi, "Dispersion and deposition of spherical particles from point sources in a turbulent channel flow," Aerosol Sci. Technol. **16**, 209–226 (1992).
[18]P. Costa, "A FFT-based finite-difference solver for massively-parallel direct numerical simulations of turbulent flows," Comput. Math. Appl. **76**, 1853–1862 (2018).
[19]H. Ounis, G. Ahmadi, and J. B. McLaughlin, "Brownian diffusion of submicrometer particles in the viscous sublayer," J. Colloid Interface Sci. **143**, 266–277 (1991).
[20]C. Marchioli, A. Soldati, J. Kuerten, B. Arcen, A. Tanière, G. Goldensoph, K. Squires, M. Cargnelutti, and L. Portela, "Statistics of particle dispersion in direct numerical simulations of wall-bounded turbulence: Results of an international collaborative benchmark test," Int. J. Multiphase Flow **34**, 879–893 (2008).
[21]F. Picano, G. Sardina, and C. M. Casciola, "Spatial development of particle-laden turbulent pipe flow," Phys. Fluids **21**, 093305 (2009).
[22]We note that the same trend in accelerations was observed for the other particle sizes ($d_p = 1$ and 5 μm), therefore those results are not presented here to avoid redundancy.
[23]J. Young and A. Leeming, "A theory of particle deposition in turbulent pipe flow," J. Fluid Mech. **340**, 129–159 (1997).
[24]Y. Li, J. B. McLaughlin, K. Kontomaris, and L. Portela, "Numerical simulation of particle-laden turbulent channel flow," Phys. Fluids **13**, 2957–2967 (2001).
[25]J. K. Eaton, "Two-way coupled turbulence simulations of gas-particle flows using point-particle tracking," Int. J. Multiphase Flow **35**, 792–800 (2009).
[26]P. L. Johnson, M. Bassenne, and P. Moin, "Turbophoresis of small inertial particles: Theoretical considerations and application to wall-modelled large-eddy simulations," J. Fluid Mech. **883**, A27 (2020).
[27]T. J. Boerner, S. Deems, T. R. Furlani, S. L. Knuth, and J. Towns, "ACCESS: Advancing innovation: NSF's advanced cyberinfrastructure coordination ecosystem: Services & support," in *Practice and Experience in Advanced Research Computing 2023: Computing for the Common Good, PEARC'23 No. 4* (Association for Computing Machinery, New York, 2023), pp. 173–176.